Title
Emergent properties of organic matter decomposition by soil enzymes

Authors
Wang, B
Allison, SD

Publication Date
2019-09-01

DOI
10.1016/j.soilbio.2019.107522

Peer reviewed

Emergent properties of organic matter decomposition by soil enzymes

Bin Wang [1], Steven D. Allison [1,2]

[1] Department of Ecology and Evolutionary Biology, University of California, Irvine, CA

[2] Department of Earth System Science, University of California, Irvine, CA

Abstract

Plant residues and soil organic matter are predominantly decomposed by exoenzymes. Many soil carbon models now represent enzymatic decomposition, but the mathematical formulation of this process has been debated over the last 15 years. Some models apply the traditional "forward" Michaelis-Menten equation to represent enzyme kinetics, whereas others apply the "reverse" Michaelis-Menten equation, which assumes that kinetic rates saturate at high enzyme concentrations. Recently the equilibrium chemistry approximation (ECA) has been proposed as an alternative to both Michaelis-Menten formulations. However, because of methodological limitations, *in-situ* enzyme kinetics—especially in the context of soil system heterogeneity—have been difficult to verify experimentally. Therefore, the overarching goal of our study was to evaluate different enzyme kinetic formulations using model-based evidence at microbial to ecosystem scales. We used a spatially explicit individual- and trait-based microbial model, DEMENT, to circumvent methodological challenges. Although DEMENT assumes forward Michaelis-Menten kinetics at local scales, at the grid scale we found saturating relationships between degradation rate and both substrate concentrations and enzyme concentrations that fit the forward and reverse Michaelis-Menten equations, respectively, at specific successional stages during decomposition. Although forward and reverse Michaelis-Menten equations emerged under some conditions, only the ECA adequately represented decay rates emerging from the spatial-temporal variation in substrate and enzyme concentrations throughout the decomposition process. Our results support a more widespread adoption of the ECA equation in soil biogeochemical modelling at ecosystem scales.

Keywords: Soil heterogeneity; Microbe; Enzyme; Trait-based model; Michaelis-Menten; Equilibrium chemistry approximation (ECA)

1. Introduction

Decomposition of plant residues and soil organic matter is a fundamental process of regenerating compounds that can be used by plants and microbes. Carbon dioxide release by decomposition is integral to biosphere-atmosphere interactions in the Earth system. Exoenzymes influence this decomposition process by catalyzing substrate transformations (e.g., Sinsabaugh et al. 2008), although a variety of non-microbial processes can also contribute (Wang et al. 2017). Because enzymes are responsible for substrate degradation, an intuitive question thus arises: what is the relationship between organic matter decomposition rate and enzyme concentration? This kinetic relationship is critical for modeling decomposition rates and fluxes of carbon and nutrients between the biosphere and atmosphere.

Studies relating decomposition of organic matter/plant detritus to many environmental factors have a long history since the early 1930s (see reviews of Manzoni and Porporato 2009; Campbell and Paustian 2015; and Wieder et al. 2015). However, an integration of enzymes into the quantitative representation of decomposition did not exist until the early 1990s. Until then, first-order equations were used with relatively little attention to microbial activity and enzymes [but see Parnas (1975)]. Even in the early stages of accounting for enzymes, first-order equations derived from empirical relationships of decay versus enzyme activity were used (e.g., Sinsabaugh et al. 1992, 1994; Moorhead et al. 1996).

A more mechanistic description was borrowed from the enzymatic chemistry field as proposed by Michaelis and Menten (1913):

$$V = \frac{k_{cat} E_0 S_0}{K_m + S_0} \quad (1)$$

where E_0 and S_0 represent enzyme and substrate concentration, respectively, k_{cat} represents the enzyme catalytic constant, and K_m denotes the concentration of S at which V is one half V_{max}. It is noteworthy that the earliest applications of the Michaelis-Menten relationship in microbial decomposition date back to the 1940s describing microbial growth in chemostats (Monod 1942). This relationship has now become commonly applied to the kinetics of enzyme-driven soil organic matter degradation (e.g., Roberts 1977; Manzoni and Porporato 2009; Wieder et al. 2015).

However, debate has arisen over the application of the Michaelis-Menten equation since the proposal of the so-called 'reverse' Michaelis-Menten equation by Schimel and Weintraub in 2003 for soil carbon and nitrogen modeling:

$$V = \frac{k_{cat} S_0 E_0}{K_m + E_0} \quad (2)$$

'Reverse' refers to the reaction rate saturating with increasing enzyme instead of substrate as in the forward equation. This modification is based on Langmuir adsorption isotherm theory which posits that that substrate binding sites may become limiting as enzyme concentration increases (Schimel and Weintraub 2003). To address a similar issue, the reverse equation has been suggested in the field of catalytic chemistry as well (e.g., Borghans et al. 1996; Tzafriri 2003; Bajzer and Strehler 2012; Kari et al. 2017). Over the past decade, researchers have proposed additional applications of the reverse equation (e.g., Moorhead et al. 2012; Sulman et al. 2014; Wieder et al. 2015) and conducted theoretical explorations of its rationale in soil organic matter modeling (e.g.,

92 Wang and Post 2013; Tang 2015; Moorhead and Weintraub 2018). Over the past 15 years,
93 biogeochemical models with different objectives and scales have applied one of the two equations
94 depending on their developers' preferences and perspectives (see review by Wieder et al. 2015).
95 Recently, Tang and Riley (2013) proposed a third formulation of enzyme kinetics known
96 as the equilibrium chemistry approximation (ECA):
97
98 $$\boldsymbol{V = \frac{k_2\, S\, E}{k_m + S + E}} \quad \textbf{(3)}$$
99
100 where k_2 and k_m refer to the maximum product genesis rate and the Michaelis-Menten constant,
101 respectively. Tang and Riley (2013) derived the ECA from the first-order approximation of the
102 full equilibrium chemistry formulation of a consumer–substrate network that can account for
103 multiple consumers and multiple substrates. The ECA has been argued to be more general and
104 therefore preferable to forward or reverse Michaelis-Menten kinetics (Tang 2015). Still, selecting
105 the best kinetic model in soil organic matter modelling has been hindered due to the difficulty of
106 measuring enzyme kinetics under in-situ soil conditions, which are very heterogeneous in space
107 and time.
108 To circumvent these limitations, we used a spatially explicit individual- and trait-based
109 microbial modelling framework, DEMENT (Allison 2012), to analyze enzyme kinetic equations
110 in the context of simulated spatial-temporal heterogeneity. With this model-based evidence, we
111 find, for the first time, that in addition to being a more general kinetic formulation, the ECA (**Eq.3**)
112 is best able to represent substrate degradation rates emerging from heterogeneous soil
113 environments. This result offers promise that the ECA equation could be widely adopted for
114 simulating large-scale soil organic matter decomposition in Earth system models.

2. Methods

2.1. Model description

DEMENT (DEcomposition Model of ENzymatic Traits) is a spatially explicit individual- and trait-based microbial model that simulates litter decomposition as an outcome of the emergent behavior of microbial systems integrating processes from both individual cell-level physiology and community-level interactions (Allison 2012). A microbial community composed of multiple taxa can be initiated with a random distribution on a spatial grid. In our study, the grid is 100 x 100, with each grid box approximately 1-10 μm on a side. During an explicit simulation of physiological metabolism and ecological interactions, microbes grow, die, reproduce, and disperse on the grid. Physiology is governed by trait distributions and tradeoffs, for example among enzyme production rate and enzyme kinetic parameters. Taxa produce constitutive and inducible enzymes as a fraction of standing biomass and resource uptake, respectively. These enzymes explicitly degrade substrates of different types following the rule that all enzymes degrade at least one substrate and all substrates are degraded by at least one enzyme. Substrate degradation rates are calculated within each grid box using the forward Michaelis-Menten equation (**Eq.1**). A more detailed description and applications of this model are referred to Allison (2012) and Allison and Goulden (2017). The required input parameters of this model are listed in **Table A1** in the **Appendix**. The source code of the DEMENT version used in this study written in the R programming language is available on GitHub (https://github.com/stevenallison).

2.2. Modelling setup and experiments

We set up DEMENT with only one bacterial taxon (simplifying the kinetic analysis from disturbances including ecological interactions) and specified an occupancy probability of 0.01 in each grid box of the 100×100 spatial grid. Following random placement of bacterial cells, 109 grid boxes were occupied by the taxon which produced a maximum of 30 different enzymes. Substrates (12 types in total including dead microbes and inactivated enzymes; see **Table A2** in the **Appendix** for their initial amounts) were initialized homogeneously on the spatial grid to be decomposed by the taxon with different enzymes.

With the setup of DEMENT as described above, a series of enzyme manipulation simulations were conducted. Because enzyme production rates can vary across ecosystems, microbial taxa, and environmental conditions, we tested the model sensitivity to varying rates of constitutive and inducible enzyme production (expressed by parameters of EnzProdConstit and EnzProdInduce in the model, respectively; see **Table A3** in the **Appendix** for a list of simulated rates). All simulations with differing enzyme production rates were driven by a constant temperature of 15 °C without water stress for 300 days (long enough to see dramatic system changes in substrate and enzyme concentrations). All other parameter values are listed in **Table A1** in the **Appendix**.

2.3. Data analyses

Using the simulation outputs, we analyzed substrate degradation rates as a function of substrate and/or enzyme concentration. Note that different substrates were targeted by different enzymes but showed qualitatively similar spatial and temporal patterns of degradation. Also, different enzyme production rates did not alter the qualitative patterns of substrate degradation.

Therefore, we selected cellulose dynamics at an intermediate enzyme production rate (15×10^{-5} mg C mg^{-1} day^{-1} for both constitutive and inducible production) for comprehensive analyses of enzyme kinetic relationships.

To determine how well enzyme kinetic equations captured substrate degradation rates at the whole grid scale, simulation data from every grid box on three different days (140, 160, and 200; chosen to capture the temporal variation) were extracted to examine relationships between degradation rate and both substrate and enzyme concentration by fitting the forward equation (**Eq.1**), the reverse equation (**Eq.2**), or the ECA equation (**Eq.3**). To further examine the overall performance of the different equations, a 'time-for-space' substitution approach was applied by plotting all points together from 5 different days (40, 80, 120, 160, and 200, each representing a different stage in the successional trajectory of substrate decay) to examine the relationship between degradation rate and both substrate and enzyme concentrations. Lastly, cellulose degradation rate and substrate and enzyme concentrations averaged over the spatial grid on each day were used to examine the degradation rate as a function of both substrate and enzyme concentrations (summed over the 3 enzymes shown in **Table A4** in the **Appendix**). These data were fitted with the ECA equation (**Eq.3**).

All non-linear regression analyses in this study were completed by obtaining the best fit between DEMENT output data and corresponding models (**Eq.1-3**) using a nonlinear least-squares approach with the Gauss-Newton algorithm of the *nls()* function in the R programming language. We calculated RMSE (root mean squared error) to quantify model fit.

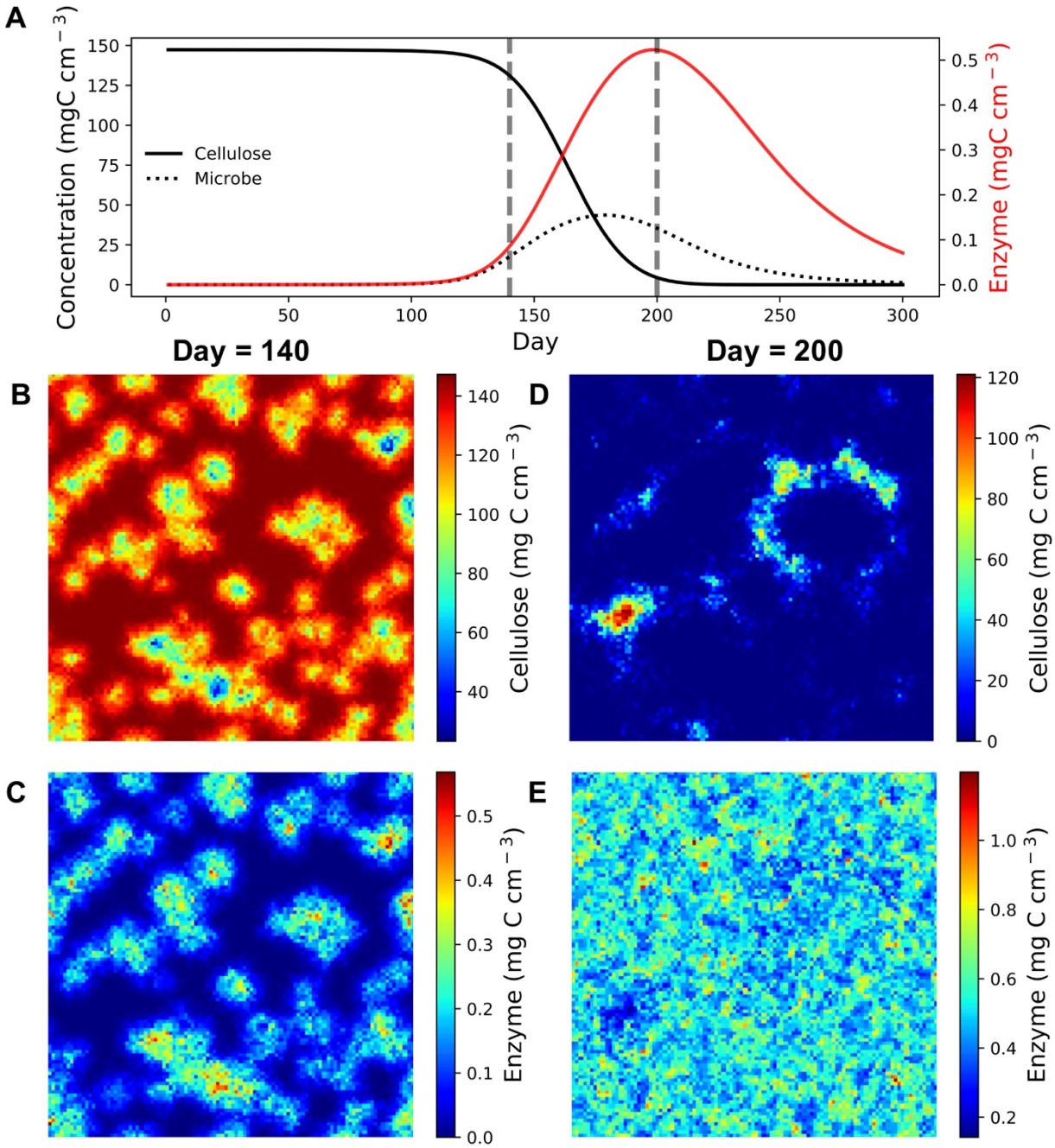

182

183 **Fig.1 Temporal dynamics and spatial pattern of cellulose and corresponding enzyme**
184 **abundance on the 100×100 spatial grid. A**) the temporal dynamics of cellulose and enzyme
185 concentrations averaged over the spatial grid, as well as the trajectory of mean microbial biomass
186 density, over 300 days with enzyme production rates of 15×10^{-5} mg C mg^{-1} day^{-1} for both

constitutive and inducible production. Spatial distributions are shown for day 140 (**B, C**) and day 200 (**D, E**). Note three different enzymes are responsible for the degradation of cellulose in the simulation (see kinetic parameters in **Table A4** in the **Appendix**).

3. Results

3.1. Spatial pattern and temporal dynamics of substrate and enzymes

Cellulose—our example substrate—declined gradually until around day 120 when its concentration started to decline sharply before nearly disappearing over the next 80 days (**Fig.1A**). In contrast, enzyme concentrations lagged behind biomass to reach a peak value of ~ 0.5 mg C cm^{-3} on day 200, after which the enzyme concentrations started to decline (**Fig.1A**). The enzyme peak lags the biomass peak because high inducible enzyme production happens after increased monomer uptake from the biomass-driven peak in constitutive enzyme production. On day 140, the cellulose concentration varied from <40 to ~140 mg C cm^{-3}, whereas the enzyme concentration ranged from zero to as high as ~0.5 mg C cm^{-3} (**Fig.1B,C**). A maximum biomass:substrate ratio of 2631.733 was reached on day 281, and a maximum enzyme:biomass ratio of 0.055 was reached on day 300. Locally high enzyme concentrations resulted in substrate 'holes' with low substrate concentrations. These 'holes' deepened and expanded (**Fig.1D**) as enzymatic degradation increased (**Fig.1E**). Over time, reproduction and dispersal of microbial cells across the grid led to an expansion of areas with high enzyme concentrations.

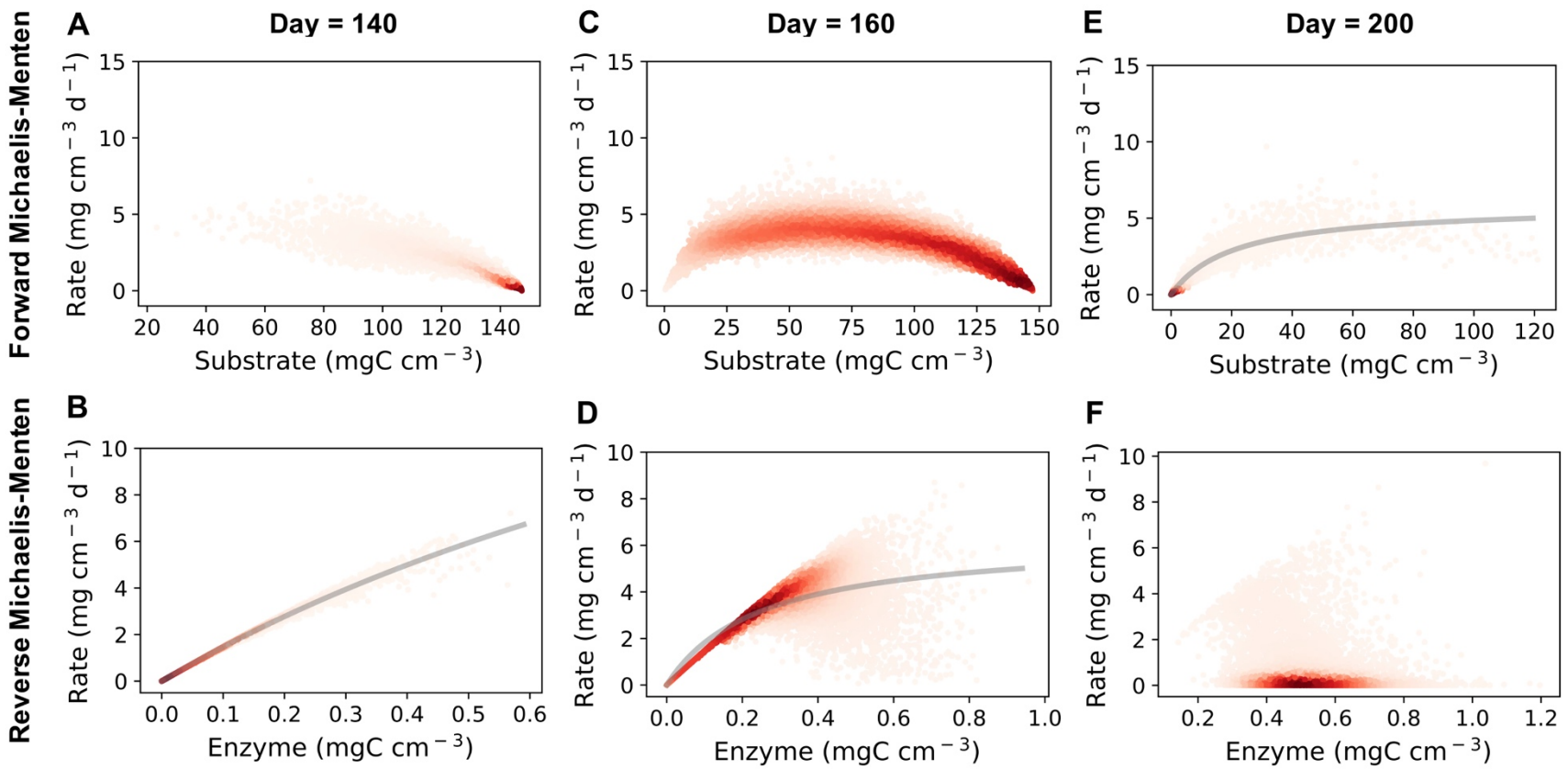

208

209 **Fig.2 Degradation rate versus enzyme and substrate concentration over the 100×100 spatial grid on different days**. Data shown
210 are extracted from every grid box on days 140, 160, and 200. High intensity of color denotes higher density of points based on kernel
211 density distribution. Lines in **B** (Vmax: 24.895 mg substrate mg^{-1} enzyme d^{-1}; Km: 1.595 mg cm^{-3}) and **D** (Vmax: 6.324 mg substrate
212 mg^{-1} enzyme d^{-1}; Km: 0.248 mg cm^{-3}) show the best fits of the reverse equation (**Eq.2**), whereas **E** (Vmax: 5.862 mg substrate mg^{-1}
213 enzyme d^{-1}; Km:20.781 mg cm^{-3}) shows the best fit of the forward equation (**Eq.1**). Neither model fits in **A**, **C**, and **F**.

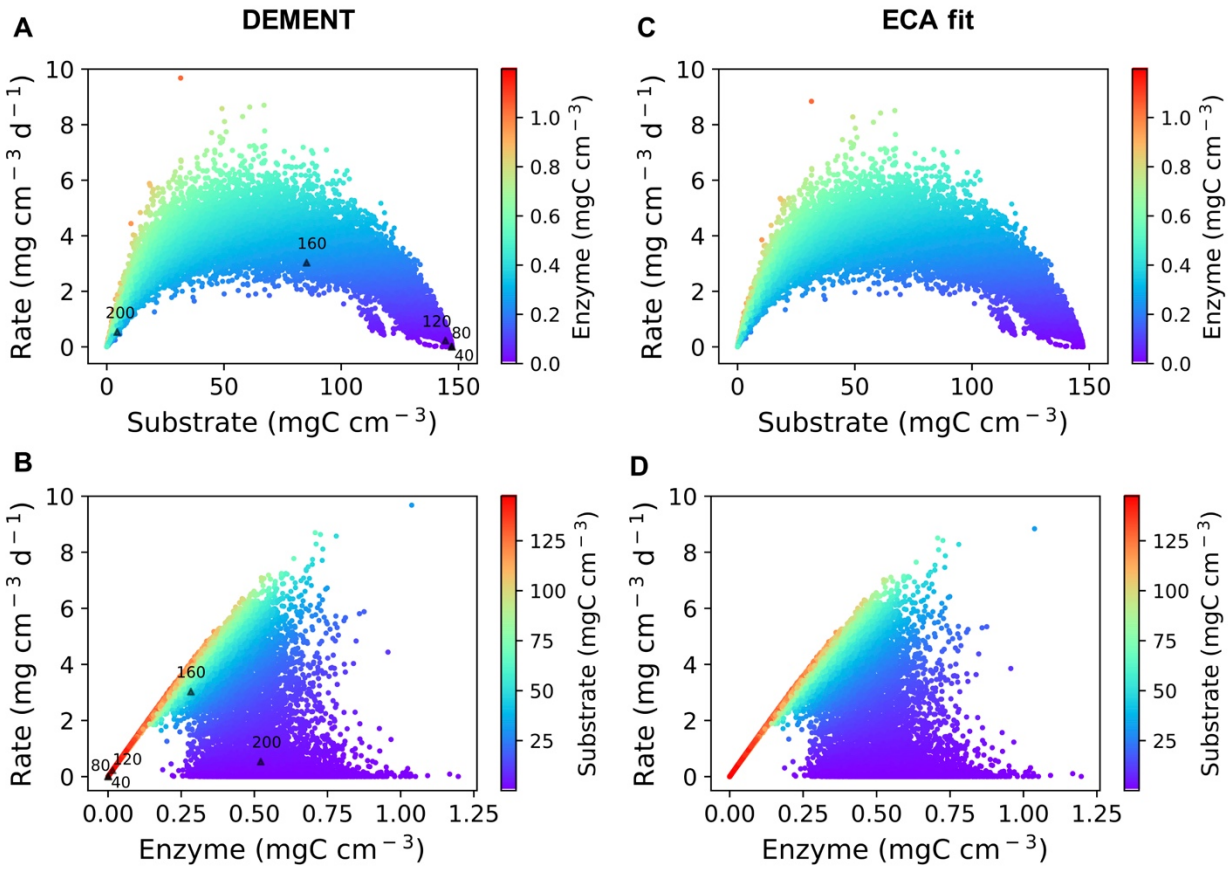

Fig.3 Degradation rate versus substrate and enzyme concentration over the 100×100 spatial grid with data from specific dates plotted together. Points in **A, B** represent grid box data on days 40, 80, 120, 160, and 200 from the simulation with enzyme production rates of 15.0×10^{-5} mg C mg^{-1} day^{-1} (both constitutive and inducible). Black triangles denote the means for each day. Panels **C, D** show the best fit of the ECA equation (**Eq.3**) to data from panels **A** and **B**, with k_2 = 18.722 mg substrate mg^{-1} enzyme d^{-1} and k_m = 36.722 mg cm^{-3} (RMSE = 0.026 mg cm^{-3} d^{-1}). Different colors denote enzyme (**A,C**) or substrate concentration (**B,D**).

3.2. Relationships between rates and enzyme/substrate concentrations over the spatial grid

To test the applicability of the forward and reverse equations, the relationships between degradation rate and both enzyme and substrate concentrations over the spatial grid were analyzed

on selected days by fitting the forward equation (**Fig.2A,C,E**) or reverse equation (**Fig.2B,D, F**). On day 140, the reverse equation provided a good fit to substrate degradation rates (**Fig.2B**), whereas the forward equation did not (**Fig.2A**). By day 160, the reverse equation fit the degradation rate to some extent (**Fig.2D**), while the forward equation apparently did not (**Fig.2C**). By day 200, the forward equation fit the substrate degradation rate (**Fig.2E**), whereas the reverse equation did not (**Fig.2F**).

When spatial data were combined across time from four selected days (**Fig.3**), most of the data points clustered around areas with high substrate concentrations (nearly 150 mgC cm^{-3}) and near-zero rate (from early in the simulation) or around areas of fairly low substrate concentration and rate (from late in the simulation) (see **Fig.A1A** for the density of these data points). For rate versus enzyme, most of the data points clustered around areas with low enzyme concentrations and decay rates (from the early stage of the simulation) or around areas with moderate enzyme concentration (around 0.6 mgC cm^{-3}) and zero degradation rates (later in the simulation) (see **Fig.A1B** for the density of these data points). With these combined data from multiple days, both the reverse and forward equations failed to capture most of the spatial variation across the grid or even the daily grid averages (**Fig.3A,B)**. Specifically, the reverse equation failed to capture the low average degradation rate on day 200, and the forward equation failed to capture low average values early in the simulation (days 40-120). In contrast, the ECA equation performed very well in capturing spatial and temporal variation in the degradation rate (**Fig.3C,D**).

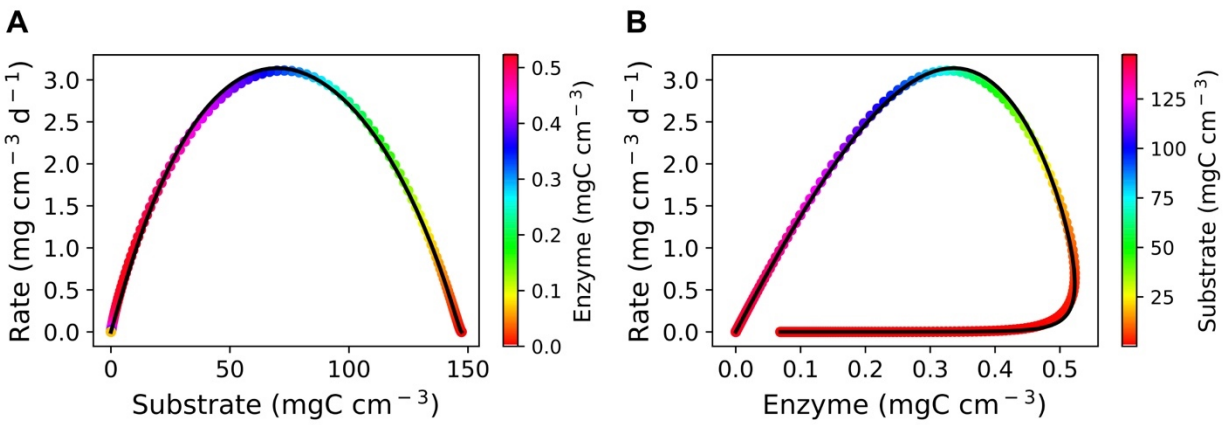

Fig.4 Cellulose degradation rate as a function of both substrate and enzyme concentration following the ECA model. A) degradation rate versus substrate concentration and **B**) enzyme concentration. Points in color represent averages over the grid for each day with colors denoting enzyme (**A**) or substrate concentration (**B**). Black line follows the fitted ECA equation with k_2 = 30.7 mg substrate mg^{-1} enzyme d^{-1} and k_m = 158.6 mg cm^{-3} (RMSE = 0.028 mg cm^{-3} d^{-1}).

3.3. Degradation as a function of both substrate and enzyme concentrations following the ECA model

All cellulose data from each day were averaged over the spatial grid and fitted with the ECA model (**Fig.4**). The degradation rate varied significantly with substrate concentration, forming a 'hump-shaped' pattern (**Fig.4A**), consistent with **Fig.3A** (which shows grid box-specific data from 5 days of a single simulation**)**. Similarly, the degradation rate varied significantly with enzyme concentration, forming a 'closed circle' pattern because of a consistent temporal depletion of substrates (**Fig.4A**), also evident in **Fig.3B**. It is noteworthy that at the same enzyme concentration, the degradation rate varied because of the temporal variability in substrate concentration. The ECA equation captured this variation in degradation rate very well as a function of both substrate and enzyme concentration (**Fig.4**). The fit of the ECA was robust to variation in

the enzyme production rate (**Fig.A2** in the **Appendix**). The ECA fit was also robust across substrates (**Fig. A3** and **Table A5** in the **Appendix**).

4. Discussion

4.1. Spatial and temporal variation in substrate degradation rates

Soil systems are highly heterogeneous and dynamically changing; substrate availability, microbial activities, and thereby enzymes are not well-mixed in the soil matrix (e.g., Young and Crawford 2004; Lowery and Ursell 2018). This heterogeneity results from many physical, chemical, and biological factors including, among others, residue input heterogeneity, physical protection by minerals and aggregation (e.g., Six et al. 2004; Wang et al. 2019), and priming (e.g., Kuzyakov 2010; Drake et al. 2011). All of these factors contribute to the dynamic, complex interactions of microbial populations and substrate availability, producing heterogeneous degradation in the soil matrix. As in real soil environments, our simulations reflected heterogeneous changes in degradation both temporally and spatially (**Fig.1**). Microbes were not uniformly distributed at the onset of simulations, and this heterogeneity was reinforced through reproduction and dispersal. Although DEMENT does not represent all mechanisms leading to heterogeneity in soils, variation in microbial densities was sufficient to drive substantial heterogeneity in substrate concentrations, enzyme concentrations, and degradation rates.

4.2. New kinetic relationships emerge from the forward equation

At the biochemical level, all of our simulations assume forward Michaelis-Menten kinetics for enzyme reactions at a local scale. Within each grid box at a given time step, enzyme and substrate concentrations are assumed to be well-mixed and at steady state. However, at the grid

scale and across time steps, these assumptions do not hold (**Fig.2**). When new substrates are introduced to an ecosystem, microbial population sizes and enzyme concentrations are low. Microbial cells and enzymes are spatially separated from substrate patches; many patches with high substrate concentrations have zero rates because no enzymes are present locally. Later in the decomposition process, substrate concentrations can decline rapidly, particularly where microbes secrete enzymes and grow rapidly. Within these substrate "holes", the degradation rate per volume or area declines. Therefore the mathematical formulation and parameters used at the scale of a grid box, or applied in a laboratory assays, should not be expected to apply at whole-grid or ecosystem scales.

Still, under certain conditions, emergent kinetics at the grid scale appear to follow the forward or reverse Michaelis-Menten relationships. Early in the decomposition process (**Fig. 2B**), the degradation rate follows a pseudo-linear increase with enzyme concentration across grid boxes. But as enzyme concentrations increase further, enzymes become locally limited by substrate availability which causes the degradation rate to level off (**Fig.2D**). The reverse equation emerges from the local forward kinetics during the early stages of decomposition before substrates become locally depleted. In our simulations, low-enzyme, high substrate conditions persisted for 100-150 days, consistent with a lag in bacterial population growth. Such lags also occur in microcosm experiments during the establishment of pure cultures on sterile, complex substrates (Taylor et al. 1989). In the DEMENT model, lag periods decline as enzyme production rates increase (**Fig.A2**).

It is noteworthy that this spatial mechanism of rate saturation with enzyme is different from biochemical enzyme kinetics. Biochemically, the reverse equation builds on the assumption of quasi-stationary substrate concentrations, where this assumption is fulfilled for insoluble substrates (interfacial reactions) on which new binding sites are consistently made available to

311 enzymes during degradation (Kari et al. 2017; Andersen et al. 2018). Recently, with cellulose-
312 cellulase as an example system, Kari et al. (2017) showed that the reverse equation is a more
313 applicable kinetic model for enzyme-driven reactions of insoluble substrates.

314 Later in decomposition, steep declines in substrate concentrations and higher enzyme
315 concentrations (**Fig.1**) lead to an emergent forward Michaelis-Menten relationship driven by
316 spatial variation (**Fig.2E**). This apparent relationship arises because substrate locally limits
317 microbial activity and enzyme production. Substrate 'holes' have been established long enough
318 for local cell populations to crash and enzyme concentrations to decline. Patches of remaining
319 substrate support higher levels of enzyme production and decay. The timing of emergence for the
320 forward Michaelis-Menten relationship along with the apparent parameters likely depend on
321 enzyme turnover rates (**Table A1**). In DEMENT, these rates are based on empirical data (Allison
322 2006).

323

324 **4.3. ECA captures kinetics emergent from spatial and temporal variation**

325 Our results show that neither the forward nor the reverse equation can fully describe
326 enzymatic degradation rates in soils (**Fig.2,3**), whereas the ECA equation is capable of capturing
327 the patterns in substrate degradation over time and space (**Fig.3,4**). Superficially, this equation
328 makes a very simple linkage to both the forward and reverse equations: when enzyme
329 concentration is low relative to substrate, the equation converges on forward Michaelis-Menten
330 kinetics; when substrate concentration is low relative to enzyme, the equation converges on the
331 reverse equation. Mechanistically, this equation can be derived from the forward and reverse
332 equations based on the law of mass action and the assumption of a quasi-steady state for the
333 enzyme–substrate complex (Tang 2005; Andersen et al. 2018). Therefore, Tang (2015) concluded

that the forward and reverse Michaelis-Menten equations are just two special cases of the ECA based on an analytical analysis. In fact, a similar kinetic description arising from systematic depletion of enzyme and substrate was proposed decades ago by Cha and Cha (1965). Our analyses extend this framework to include apparent kinetics emergent from spatial and temporal variation in enzyme and substrate concentrations, which should be broadly applicable for scaling up microbial processes to the ecosystem scale. This emergence of a coarse-scale pattern from local-scale kinetics is analogous to results from a cell population study by Chaplain et al. (2018), who found that an individual-based model can generate complex spatial patterns of population growth observed in a corresponding continuum model.

4.4. Broder implications for developing soil biogeochemical models

Our study can help develop soil biogeochemical models that more accurately simulate microbe-driven organic matter decomposition and evaluate soil-atmosphere interactions. The spatial and temporal variation in soil systems represents one of the biggest challenges in achieving this goal. To this end, a method for scaling up local heterogeneity is required for large scale modeling. Neither reverse nor forward Michaelis-Menten kinetics are sufficient for this scaling, which may explain the large uncertainties in soil carbon dynamics observed within and across soil carbon models [see the synthesis study by Sulman et al. (2018)]. Our study suggests that the ECA equation is suitable for this scaling process and can be incorporated into land surface and Earth system models (Huang et al. 2018; Riley et al. 2018). ECA parameters can be derived by fitting spatially-explicit model output at the microbial scale (**Table A3, A5**).

At the same time, a broader application of the ECA requires more attention to the representation of enzymes in ecosystem models. Most current models simulate the enzyme pool

357 implicitly as a function of microbial biomass [see the review by Wieder et al. (2015)]. The ECA
358 may require more explicit parameterizations of enzyme production and activity, a gap that requires
359 more research.

360 Our study might be generalizable beyond soil systems. Applications of the Michaelis-
361 Menten equation are ubiquitous [e.g., see Table 1 in Wong et al. (2018)], and scaling up the
362 associated processes is a common concern in heterogeneous systems. For example, microbe-driven
363 element cycling in marine systems faces a similar problem of heterogeneity (e.g., Follows et al.
364 2007; Ward et al. 2014; Moradi et al. 2018), and we speculate that an application of the ECA
365 equation (not necessarily the exact same parameter meaning) could help address this challenge. In
366 forest systems, a landscape mosaic of forest gaps at differing stages (Shugart 1984) could benefit
367 from a similar application of the ECA equation in a different form.

368

369 **5. Conclusions**

370 Our model-based analyses shed light on the uncertainty surrounding the enzyme kinetics
371 of litter and soil organic matter decomposition. Specifically, our study shows that both forward
372 and reverse Michaelis-Menten relationships can emerge at the ecosystem scale from local-scale
373 biochemical kinetics. However, these formulations fail to capture the full range of decay rate
374 dependencies on substrate and enzyme concentrations. This inconsistency arises from soil system
375 heterogeneity over space and time that cannot be captured by a single forward or reverse equation.
376 In contrast, we demonstrate that the ECA equation can represent the emergent spatial and temporal
377 heterogeneity in soil substrate degradation. We expect that adopting this more general equation in
378 building biogeochemical and Earth system models would contribute to greater accuracy in
379 simulating soil carbon metabolism over large scales of time and space.

Acknowledgement

All source data and code (in the format of Jupyter Notebook showing step-by-step analyses written in Python or R) in producing the figures in this manuscript are archived on GitHub (https://github.com/bioatmosphere/An_emergent_soil_enzyme_decomposition_model). The US Department of Energy, Office of Science (BER), funded this research through grants DE-SC0014374 and DE-SC0016410.

References

Allison, S. D., 2006. Soil minerals and humic acids alter enzyme stability: implications for ecosystem processes. Biogeochemistry, 81, 361-373.

Allison, S. D., 2012. A trait-based approach for modelling microbial litter decomposition. Ecology Letters, 15, 1058-1070.

Allison, S. D., Goulden, M. L., 2017. Consequences of drought tolerance traits for microbial decomposition in the DEMENT model. Soil Biology and Biochemistry, 107, 104-113.

Andersen, M., Kari, J., Borch, K., & Westh, P., 2018. Michaelis-Menten equation for degradation of insoluble substrate. Mathematical Biosciences, 296, 93-97.

Bajzer, Ž., Strehler, E. E., 2012. About and beyond the Henri-Michaelis−Menten rate equation for single-substrate enzyme kinetics. Biochemical and Biophysical Research Communications, 417, 982−985.

Borghans, J. A., De Boer, R. J., Segel, L. A., 1996. Extending the quasi-steady state approximation by changing variables. Bulletin of Mathematical Biology, 58, 43-63.

Cha, S., Cha, C. J. M., 1965. Kinetics of cyclic enzyme systems. Molecular Pharmacology, 1, 178-189.

Chaplain, M. A., Macfarlane, F. R., Lorenzi, T., 2018. Bridging the gap between individual-based and continuum models of growing cell populations. arXiv preprint arXiv:1812.05872.

Drake, J.E., Gallet-Budynek, A., Hofmockel, K.S., Bernhardt, E.S., Billings, S.A., Jackson, R.B., Johnsen, K.S., Lichter, J., McCarthy, H.R., McCormack, M.L., Moore, D.J., 2011. Increases in the flux of carbon belowground stimulate nitrogen uptake and sustain the long-term enhancement of forest productivity under elevated CO_2. Ecology Letters, 14, 349-357.

Huang, Y., Guenet, B., Ciais, P., Janssens, I. A., Soong, J. L., Wang, Y. L., Goll, D., Blagodatskaya, E., and Huang, Y. Y., 2018. ORCHIMIC (v1.0), a microbe-mediated model for soil organic matter decomposition. Geoscientific Model Development, 11, 2111-2138.

Kari, J., Andersen, M., Borch, K., Westh, P., 2017. An Inverse Michaelis–Menten Approach for Interfacial Enzyme Kinetics. Acs Catalysis, 7, 4904-4914.

Kuzyakov, Y., 2010. Priming effects: Interactions between living and dead organic matter. Soil Biology and Biochemistry, 42, 1363-1371.

Lowery, N. V., Ursell, T., 2018. Structured environments fundamentally alter dynamics and stability of ecological communities. Proceedings of the National Academy of Sciences, 201811887.

Manzoni, S., Porporato, A., 2009. Soil carbon and nitrogen mineralization: theory and models across scales. Soil Biology and Biochemistry, 41, 1355-1379.

Michaelis, L., Menten, M.L., 1913. Die kinetik der invertinwirkung. Biochem Z, 49, 333–369.

Moorhead, D. L., Sinsabaugh, R. L., Linkins, A. E., & Reynolds, J. F., 1996. Decomposition processes: modelling approaches and applications. Science of the Total Environment, 183, 137-149.

Moorhead, D. L., Lashermes, G., & Sinsabaugh, R. L., 2012. A theoretical model of C-and N-acquiring exoenzyme activities, which balances microbial demands during decomposition. Soil Biology and Biochemistry, 53, 133-141.

445 Moorhead, D. L., Weintraub, M. N., 2018. The evolution and application of the reverse Michaelis-
446 Menten equation. Soil Biology and Biochemistry, 125, 261-262.
447
448 Moradi, N., Liu, B., Iversen, M., Kuypers, M. M., Ploug, H., & Khalili, A., 2018. A new
449 mathematical model to explore microbial processes and their constraints in phytoplankton colonies
450 and sinking marine aggregates. Science Advances, 4, eaat1991.
451
452 Parnas, H., 1975, Model for decomposition of organic material by microorganisms. Soil Biology
453 and Biochemistry, 7, 161-169.
454
455 Riley, W. J., Zhu, Q., Tang, J. Y., 2018. Weaker land–climate feedbacks from nutrient uptake
456 during photosynthesis-inactive periods. Nature Climate Change, 8, 1002-1006.
457
458 Roberts, D.V., 1977. Enzyme Kinetics, Cambridge University Press, Cambridge.
459
460 Schimel, J. P., Weintraub, M. N., 2003. The implications of exoenzyme activity on microbial
461 carbon and nitrogen limitation in soil: a theoretical model. Soil Biology and Biochemistry, 35,
462 549-563.
463
464 Schnell, S., 2014. Validity of the Michaelis-Menten equation–steady-state or reactant stationary
465 assumption: that is the question. The FEBS Journal, 281, 464-472.
466
467 Shugart, H.H., 1984. A theory of forest dynamics. Springer Verlag, New York.

Sinsabaugh, R.L., Antibus, R. K., Linkins, A. E., McClaugherty, C. A., Rayburn, L., Repert, D., & Weiland, T., 1992. Wood decomposition over a first-order watershed: mass loss as a function of lignocellulase activity. Soil Biology and Biochemistry, 24, 743-749.

Sinsabaugh, R.L., Moorhead, D.L., 1994. Resource-allocation to extracellular enzyme production: a model for nitrogen and phosphorus control of litter decomposition. Soil Biology and Biochemistry, 26, 1305-1311.

Sinsabaugh, R. L., Lauber, C. L., Weintraub, M. N., Ahmed, B., Allison, S. D., Crenshaw, C., ... Gartner, T. B., 2008. Stoichiometry of soil enzyme activity at global scale. Ecology Letters, 11, 1252-1264.

Six J, Bossuyt H, Degryze S, Denef K., 2004. A history of research on the link between microaggregates, soil biota, and soil organic matter dynamics. Soil & Tillage Research, 79, 7-31.

Sulman, B. N., Moore, J. A., Abramoff, R., Averill, C., Kivlin, S., Georgiou, K., ... & Bradford, M. A., 2018. Multiple models and experiments underscore large uncertainty in soil carbon dynamics. Biogeochemistry, 141, 109-123.

Sulman, B. N., Phillips, R. P., Oishi, A. C., Shevliakova, E., Pacala, S. W., 2014. Microbe-driven turnover offsets mineral-mediated storage of soil carbon under elevated CO_2. Nature Climate Change, 4, 1099–1102.

Tang, J. Y., 2015. On the relationships between the Michaelis–Menten kinetics, reverse Michaelis–Menten kinetics, equilibrium chemistry approximation kinetics, and quadratic kinetics. Geoscientific Model Development, 8, 3823-3835

Tang, J. Y., Riley, W. J., 2013. A total quasi-steady-state formulation of substrate uptake kinetics in complex networks and an example application to microbial litter decomposition. Biogeosciences, 10, 8329-8351

Taylor, B. R., Parkinson, D., and Parsons, W. F., 1989. Nitrogen and lignin content as predictors of litter decay rates: a microcosm test. Ecology, 70, 97-104.

Tzafriri, A. R. Michaelis-Menten kinetics at high enzyme concentrations. Bulletin of Mathematical Biology, 2003, 65, 1111−1129.

Wang, B., Brewer, P. E., Shugart, H. H., Lerdau, M. T., Allison, S. D. (2019). Soil aggregates as biogeochemical reactors and implications for soil–atmosphere exchange of greenhouse gases—A concept. Global Change Biology, 25, 373–385.

Wang, B., Lerdau, M., He, Y., 2017. Widespread production of non-microbial greenhouse gases in soils. Global Change Biology, 23, 4472-4482.

513 Wang, G., Post, W. M., 2013. A note on the reverse Michaelis–Menten kinetics. Soil Biology and
514 Biochemistry, 57, 946-949.
515
516 Ward, B. A., Dutkiewicz, S., Follows, M. J., 2013. Modelling spatial and temporal patterns in size-
517 structured marine plankton communities: top–down and bottom–up controls. Journal of Plankton
518 Research, 36, 31-47.
519
520 Wieder, W. R., Allison, S. D., Davidson, E. A., Georgiou, K., Hararuk, O., He, Y., ... & Todd-
521 Brown, K., 2015. Explicitly representing soil microbial processes in Earth system models. Global
522 Biogeochemical Cycles, 29, 1782-1800.
523
524 Wieder, W. R., Grandy, A. S., Kallenbach, C. M., Bonan, G. B., 2014. Integrating microbial
525 physiology and physio-chemical principles in soils with the MIcrobial-MIneral Carbon
526 Stabilization (MIMICS) model. Biogeosciences, 11, 3899-3917.
527
528 Wong, F., Dutta, A., Chowdhury, D., Gunawardena, J., 2018. Structural conditions on complex
529 networks for the Michaelis–Menten input–output response. Proceedings of the National Academy
530 of Sciences, 115, 9738-9743.
531
532 Young, I. M., Crawford, J. W., 2004. Interactions and self-organization in the soil-microbe
533 complex. Science, 304, 1634-1637.
534

Appendix

Emergent properties of organic matter decomposition by soil enzymes

Bin Wang [1], Steven D. Allison [1,2]

[1] Department of Ecology and Evolutionary Biology, University of California, Irvine, CA

[2] Department of Earth System Science, University of California, Irvine, CA

Table A1 Model parameter values.

Parameter	Value	Unit	Note
end_time	300		number of iterations
x	100		Grid length
y	100		Grid width
taxa_per_box	0.01		Initial probability of each bacterial taxon occupying a box
n_taxa	1		number of taxa
fb	0		Initial fraction of fungi biomass
n_enzymes	30		Number of enzymes in community
n_uptake	14		Number of uptake transporters
LCI_slope	-0.8		Fractional change in cellulose decay per unit lignocellulose index
n_substrates	12		Number of substrates
Cfrac_b	0.825	mg mg-1	Bacterial C fraction
Nfrac_b	0.16	mg mg-1	Bacterial N fraction
Pfrac_b	0.015	mg mg-1	Bacterial P fraction
Cfrac_f	0.9	mg mg-1	Fungal C fraction
Nfrac_f	0.09	mg mg-1	Fungal N fraction
Pfrac_f	0.01	mg mg-1	Fungal P fraction
Crange	0.09	mg mg-1	Tolerance on C fraction
Nrange	0.04	mg mg-1	Tolerance on N fraction
Prange	0.005	mg mg-1	Tolerance on P fraction
CUE_ref	0.5	mg mg-1	Carbon use efficiency at the reference temperature
CUE_enz	0	mg mg-1	CUE change with enzyme investment
CUE_uptake	0	mg mg-1	CUE change with uptate investment
CUE_temp	-0.016	mg mg-1 °C-1	CUE temperature sensitivity
Specif_factor	1		Efficiency-specificity
Vmax_Km	1	mg enzyme day cm-3	Slope for Km-Vmax relationship
Vmax_Km_int	0	mg cm-3	Intercept for Km-Vmax relationship
Uptake_Vmax_Km	0.2	mg biomass day cm-3	Slope for uptake Km-Vmax relationship
Uptake_Vmax_Km_int	0	mg cm-3	Intercept for uptake Km-Vmax relationship
dist	1	lattice point	Maximum dispersal distance
direct	0.95		Dispersal direction
max_size_b	2	mg cm-3	C quota threshold for bacterial cell division
max_size_f	50	mg cm-3	C quota threshold for fungal cell division
C_min	0.086	mg cm-3	threshold C concentration for cell death
N_min	0.012	mg cm-3	threshold P concentration for cell death
P_min	0.002	mg cm-3	threshold C concentration for cell death
Death_Rate	0.001		Bacterial death rate
Death_Ratio	0.2		Fungal death ratio
Enz_min	0	mg C cm-3	Initial enzyme present in terms of carbon
Enz_max	0	mg C cm-3	Initial enzyme present in terms of carbon
Enz_per_taxon_min	0		Minimum number of enzymes a taxon can produce
Enz_per_taxon_max	40		Maximum number of enzymes a taxon can produce
Enz_Prod_min	0.00001	mg C mg-1 day-1	Minimum per enzyme production cost as a fraction of C uptake rate
Enz_Prod_max	0.0001	mg C mg-1 day-1	Maximum per enzyme producton cost as a fraction of C uptakte rate
Constit_Prod_min	0.00001	mg C mg-1 day-1	Minimum per enzyme production cost as a fraction of biomass C
Constit_Prod_max	0.0001	mg C mg-1 day-1	Maximum per enzyme production cost as a fraction of biomass C
NormalizeProd	0		Normalize enzyme production for the number of enzyme genes
Enz_C_cost	1	mg mg-1	Per enzyme C cost as a fraction of uptake
Enz_N_cost	0.3	mg mg-1	Per enzyme N cost as a fraction of C cost
Enz_P_cost	0	mg mg-1	Per enzyme P cost as a fraction of C cost
Enz_Maint_cost	5	mg C mg-1 enzyme C	Maintinence cost of enzyme production
Enzyme_Loss_Rate	0.04	day-1	Enzyme turnover rate (Allison 2006)
Enzymes_per_sub	1		Minimum number of enzymes capable of degrading each substrate
Vmax0_min	5	mg substrate mg-1 enzyme day-1	Minimum Vmax for enzyme
Vmax0_max	50	mg substrate mg-1 enzyme day-1	Maximum Vmax for enzyme
Km_min	0.01	mg cm-3	Minimum Km
Km_Ea	20	kj mol-1	Activation energy for Km
NormalizeUptake	0		Normalize uptake investment for the number of uptake genes
Uptake_per_monomer	1		number of transporters per monomer
Uptake_C_cost_min	0.01	transporter mg-1 biomass C	Minimun per enzyme C cost as a fraction of uptake
Uptake_C_cost_max	0.1	transporter mg-1 biomass C	Maximum per enzyme C cost as a fraction of uptake
Uptake_Maint_cost	0.01	mg C transporter-1 day-1	Respiration cost of uptake transporters
Uptake_Vmax0_min	1	mg substrate mg-1 substrate day-1	Minimum uptake Vmax
Uptake_Vmax0_max	10	mg substrate mg-1 substrate day-1	Maximum uptake Vmax
Uptake_Ea_min	35	kj mol-1	Minimum activation energy for uptake
Uptake_Ea_max	35	kj mol-1	Maximum activation energy for uptake
Uptake_Km_min	0.001	mg cm-3	Minimum uptake Km

Table A2 Substrate concentrations initialized in DEMENT simulations (mg cm^{-3}).

Substrate	C	N	P
DeadMic	0	0	0
DeadEnz	0	0	0
Cellulose	146.89	0	0
Hemicellulose	85.855	0	0
Starch	12.21	0	0
Chitin	4.9952	0.83254	0
Lignin	48.51	0.40425	0
Protein1	10.6	2.09704	0
Protein2	10.6	2.09704	0
Protein3	10.6	2.09704	0
OrgP1	12.48	0	0.478469
OrgP2	1.8182	0.79745	0.478469

Table A3 Manipulated enzyme production rate scenarios and ECA parameter values. Bold values indicate simulations used in further analyses.

Run	EnzProdConstit	EnzProdInduce	k_2	k_m
1	2	2	17.830	28.603
2	3	3	22.353	73.208
3	4	4	21.473	65.600
4	**5**	**5**	**22.506**	**75.040**
5	6	6	22.929	80.467
6	7	7	24.091	90.833
7	8	8	22.766	81.393
8	9	9	23.244	86.231
9	**10**	**10**	**24.976**	**102.192**
10	11	11	26.746	119.165
11	12	12	26.132	114.029
12	**15**	**15**	**30.561**	**158.196**
13	17	17	32.961	180.897
14	18	18	32.575	177.935
15	**20**	**20**	**33.243**	**189.403**
16	22	22	37.327	227.398
17	25	25	41.945	273.338
18	**30**	**30**	**51.635**	**379.492**

EnzProdConstit, EnzProdInduce: 10^{-5} mg C mg^{-1} day^{-1}

k_2: mg substrate mg^{-1} enzyme d^{-1}

k_m: mg cm^{-3}

Table A4 Cellulose enzyme kinetic parameter values for the Michaelis-Menten equation.

Enzyme	Vmax(mg substrate mg^{-1} enzyme day^{-1})	Km (mg cm^{-3})
1	11.68	13.09
2	19.13	21.44
3	36.72	41.16

583

584

585

586

587

588

589

590

591

592

593

594

595

596

597

598

599

600

601

602

Table A5 ECA parameter values of different substrates based on the simulation with enzyme production rates of 15.0×10^{-5} mg C mg^{-1} day^{-1} (both constitutive and inducible).

Substrate	k_2	k_m	RMSE
Cellulose	30.561	158.196	0.029
Chitin	31.578	51.798	0.002
DeadEnz	10.027	7.717	0.004
Hemicellulose	48.030	90.618	0.019
Lignin	14.826	27.247	0.009
OrgP1	43.331	100.000	0.012
OrgP2	73.453	100.000	0.003
Protein1	35.204	100.000	0.021
Protein2	26.128	100.000	0.029
Protein3	48.722	100.000	0.011
Starch	34.229	100.000	0.016
Total	17.806	1177.599	0.178

Note: parameter values of substrates from OrgP1 through Starch are derived from fits with an upper bound of 100.0 for each parameter to avoid overfitting and should be interpreted with caution.

k_2: mg substrate mg^{-1} enzyme d^{-1}

k_m: mg cm^{-3}

RMSE: mg cm^{-3} d^{-1}

603

604

605

606

607

608

609

610

611

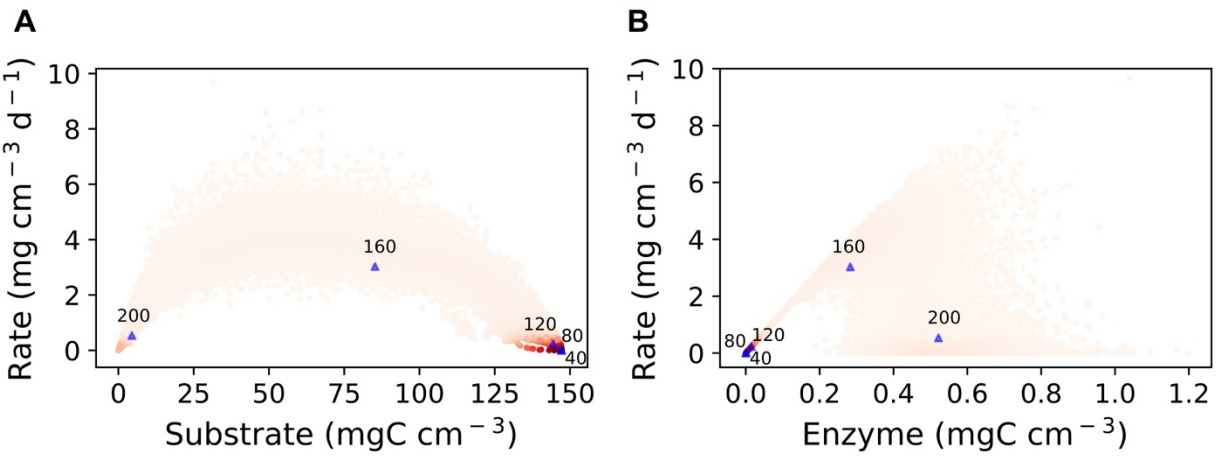

612

613 **Fig.A1 Degradation rate versus substrate and enzyme concentration over the 100×100 spatial**

614 **grid with data from specific dates plotted together.** Points represent grid box data on days 40,

615 80, 120, 160, and 200 from the simulation with enzyme production rates of 15.0×10^{-5} mg C mg^{-1}

616 day^{-1} (both constitutive and inducible). High intensity of red denotes high density of points based

617 on kernel density distribution. Blue points denote the means for each day.

618

619

620

621

622

623

624

625

626

627

628

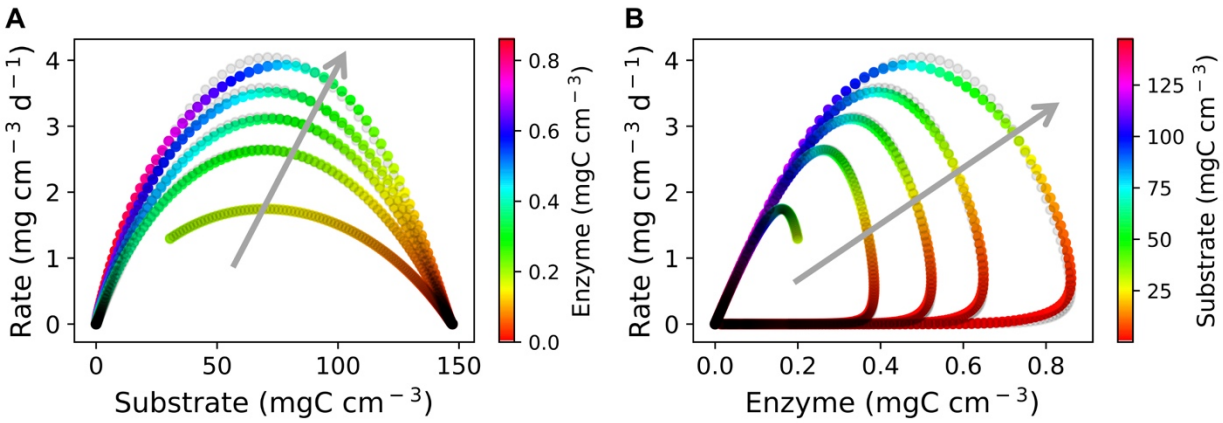

629

630

631 **Fig.A2 Cellulose degradation rate as a function of both substrate and enzyme concentration.**

632 Similar to **Fig.4**, grey points follow the best fit ECA equation (see **Table A3** for the parameter

633 values). Points in color represent averages over the grid of each day with colors denoting enzyme

634 (**A**) or substrate concentration (**B**). In contrast to **Fig.4,** the ECA equation is fitted with data from

635 five simulations with different enzyme production rates (5×10^{-5}, 10×10^{-5}, 15×10^{-5}, 20×10^{-5}, and

636 30×10^{-5} mg C mg^{-1} day^{-1}, which are selected from scenarios in **Table A3**). The arrow in grey points

637 toward increasing enzyme production rates across the simulations.

638

639

640

641

642

643

644

645

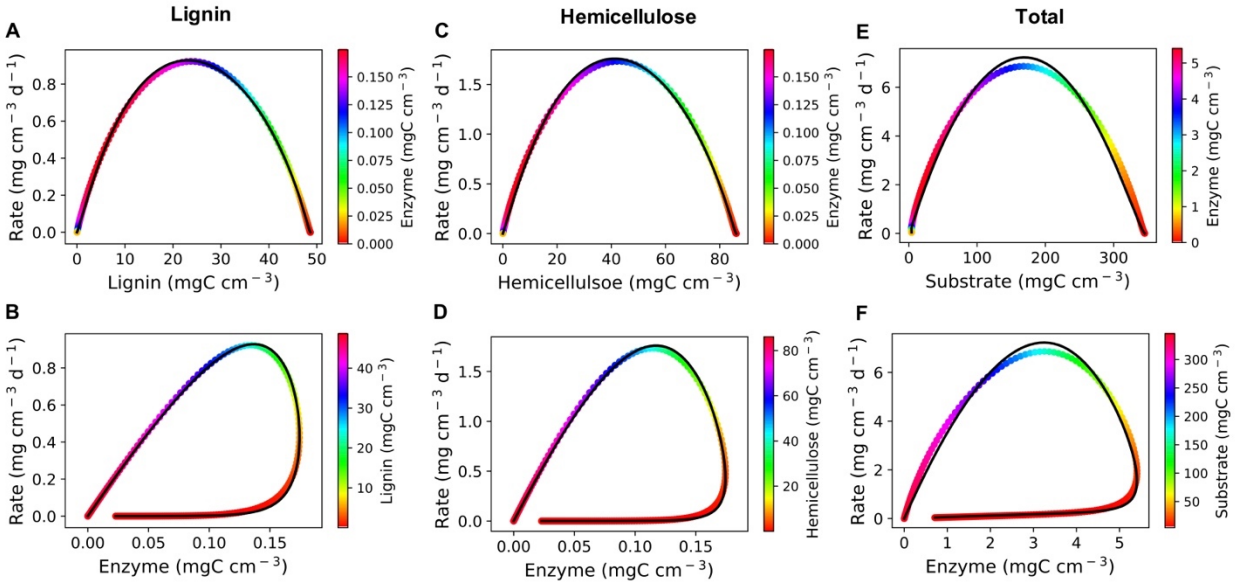

646

647

648 **Fig.A3 Same as Fig.4 but for different substrates. A,B)** Lignin (RMSE= 0.009 mg cm^{-3} d^{-1});

649 **C,D)** hemicellulose (RMSE= 0.019 mg cm^{-3} d^{-1}); and **E,F)** all substrates in the system (RMSE=

650 0.178 mg cm^{-3} d^{-1}). See **Table A5** for ECA parameter values and all other substrates.